Journal of
Synchrotron Radiation

ISSN 0909-0495

Received 30 November 2006
Accepted 27 March 2007

Energy-dispersive diffraction with synchrotron radiation and a germanium detector

Veijo Honkimäki[a]* and Pekka Suortti[a,b]

[a]European Synchrotron Radiation Facility, BP 220, F-38043 Grenoble, France, and [b]Department of Physical Sciences, PL 64, FIN-00014 Helsinki University, Finland. E-mail: honkimak@esrf.fr

The response of an intrinsic Ge detector in energy-dispersive diffraction measurements with synchrotron radiation is studied with model calculations and diffraction from perfect Si single-crystal samples. The high intensity and time-structure of the synchrotron radiation beam leads to pile-up of the output pulses, and the energy distribution of the pile-up pulses is characteristic of the fill pattern of the storage ring. The pile-up distribution has a single peak and long tail when the interval of the radiation bunches is small, as in the uniform fill pattern, but there are many pile-up peaks when the bunch distance is a sizable fraction of the length of the shaping amplifier output pulse. A model for the detecting chain response is used to resolve the diffraction spectrum from a perfect Si crystal wafer in the symmetrical Laue case. In the 16-bunch fill pattern of the ESRF storage ring the spectrum includes a large number of 'extra reflections' owing to pile-up, and the model parameters are refined by a fit to the observed energy spectrum. The model is used to correct for the effects of pile-up in a measurement with the 1/3 fill pattern of the storage ring. Si reflections $(2h,2h,0)$ are resolved up to $h = 7$. The pile-up corrections are very large, but a perfect agreement with the integrated intensities calculated from dynamical diffraction theory is achieved after the corrections. The result also demonstrates the convergence of kinematical and dynamical theories at the limit where the extinction length is much larger than the effective thickness of the perfect crystal. The model is applied to powder diffraction using different fill patterns in simulations of the diffraction pattern, and it is demonstrated that the regularly spaced pile-up peaks might be misinterpreted to arise from superlattices or phase transitions. The use of energy-dispersive diffraction in strain mapping in polycrystalline materials is discussed, and it is shown that low count rates but still good statistical accuracy are needed for reliable results.

Keywords: energy-dispersive diffraction; pile-up; high-energy X-rays.

1. Introduction

In energy-dispersive diffraction (EDD) a well collimated polychromatic beam of X-rays falls on the sample, and the spectrum of the radiation scattered at a fixed angle is analyzed (Giessen & Gordon, 1968). The analyzer is usually a solid-state detector, such as an intrinsic Ge diode, but scanning by a perfect crystal can also be used (Parrish & Hart, 1988). The principal application of the method is powder or polycrystalline diffraction, particularly under extreme conditions of high pressures and temperatures (Prewitt *et al.*, 1987; Mao & Hemley, 1998). The use of synchrotron radiation from a bending magnet or wiggler was introduced a long time ago (Buras *et al.*, 1976). With synchrotron radiation, very short data acquisition times are needed, which makes time-resolved studies of phase transitions and reaction kinetics possible (Jupe *et al.*, 1996; O'Hare *et al.*, 1998). Another application in materials science is diffraction tomography of polycrystalline samples (Hall *et al.*, 1998), and recently simultaneous absorption tomography and diffraction analysis was introduced (Pyzalla *et al.*, 2005). Creep damage can be followed *in situ*, and for high-resolution strain mapping in bulk samples the use of high-energy synchrotron radiation and EDD is superceding neutron diffraction methods. Quantitative whole-pattern refinement in powder diffraction becomes possible when the energy spectrum of the incident beam and the response function of the detecting system are known. If the sample is randomly oriented, the method can be used for solving crystal structures, and even for determining thermal parameters (Honkimäki & Suortti, 1992*b*).

The effects of high count rates have been discussed in detail recently using a pulse-overlap model for photon counting (Laundy & Collins, 2003). That work described the effects in terms of the detector dead-time, and the results are directly

applicable to the detection of mono-energetic X-rays. The present work addresses the problems encountered in EDD, where a distribution of energies is detected. The response function of a solid-state detector such as an intrinsic Ge diode involves creation of electron–hole pairs by the incident X-ray photon, charge collection, and conversion to a voltage pulse in the pre- and shaping amplifiers. The pulses are sorted into the memory of a multi-channel analyzer (MCA) after passing through an analog-to-digital converter (ADC). For a full understanding of the output signal, pulse shapes and functioning of the various components must be known in detail. The pulsed time structure of synchrotron radiation makes the temporal distribution of the output signal very non-uniform, which leads to effects that are not encountered at steady-state sources such as X-ray tubes. Unfortunately, this situation is often ignored, and the energy spectra of the scattered radiation, as recorded by solid-state detectors, are analyzed implicitly assuming a steady-state source of radiation. This article presents a direct experimental approach to the analysis of EDD patterns in single-crystal and powder diffraction, taking into account the actual time structure of the incident synchrotron radiation. The results are illustrated by several simulations and by measured diffraction patterns.

2. Pulsed source and Ge detector

A storage ring is a cyclic source of X-rays, where short bunches of electrons (or positrons) travel almost at the speed of light and emit radiation in the forward direction. The storage ring has a certain number of 'buckets', which can be filled with electrons, and this creates the so-called fill pattern. In the following we use the ESRF storage ring as an example. There the circumference of the storage ring is 844 m, and the number of buckets is 992, *i.e.* successive buckets are separated by 0.85 m in space or 2.84 ns in time. Different fill patterns are shown in Fig. 1. The partial filling modes (1/3 or 2/3) have been used to reduce ion-trapping, but recently this problem has been overcome even with the uniform fill, where all the buckets are filled. Many experiments require longer intervals between the bunches, and the fill patterns most frequently used for time-resolved experiments are the 16-bunch mode and the 1-bunch mode, where the bunch intervals are 176 ns and 2.82 µs, respectively. The RMS bunch length depends on the mode, being about 20 ps in the uniform fill and 73 ps in the 1-bunch mode. At the full current I in the storage ring, there are 3.5×10^9 electrons in a bunch with the uniform fill (I = 200 mA), 9.3×10^{10} electrons in the 16-bunch mode (I = 85 mA), and 2.6×10^{11} electrons in the single bunch orbiting in the ring (I = 15 mA).

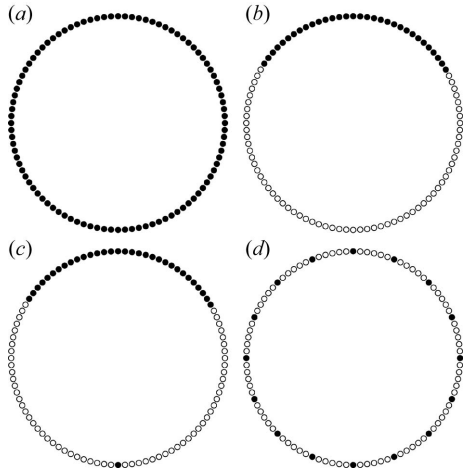

Figure 1
Fill patterns of the ESRF storage ring. There are 992 'buckets', which are spaced by 2.84 ns. In the uniform fill (*a*), all the buckets are filled by electrons; in the 1/3 fill (*b*), 2/3 of the buckets are empty; but in the hybrid mode (*c*), a single bucket in the middle of the empty part is filled. In the 16-bunch mode (*d*), the bunch interval is 176 ns.

Synchrotron radiation is emitted when the electron moves on a curved trajectory in a magnetic field. The electrons propagate almost at the same speed as the X-rays that they emit, so that the X-ray pulse is only slightly longer than the electron bunch, even when the source is an extended magnetic structure, such as a wiggler or an undulator. For the present work, it is instructive to calculate the number of X-ray photons from one bunch through a pinhole in front of the sample. The intensity at the center of the beam emitted by a bending magnet in seconds and mrad^2 within a 0.1% bandwidth is

$$\frac{\mathrm{d}^2 n}{\mathrm{d}\theta\,\mathrm{d}\psi} = 1.327 \times 10^{13}\, E^2\,[\mathrm{GeV}^2]\; I\,[\mathrm{A}]\; H_2(y), \qquad (1a)$$

$$H_2(y) = y^2 K_{2/3}^2(y/2), \qquad (1b)$$

where E is the electron energy, $y = \varepsilon/\varepsilon_c$ is the photon energy/critical energy, and $K_{2/3}$ is the modified Bessel function of the second kind. At the critical energy, $H_2(1) \simeq 1.5$, so that 5.7×10^{10} photons s^{-1} (0.1% bandwidth)$^{-1}$ of that energy pass through a 1 mm^2 pinhole placed at 50 m from the source, when E = 6 GeV and I = 0.2 A. The corresponding numbers per bunch are 1.2×10^4 photons (0.1% bandwidth)$^{-1}$ in the single-bunch mode, 4.3×10^3 photons (0.1% bandwidth)$^{-1}$ in the 16-bunch mode, and 1.6×10^2 photons (0.1% bandwidth)$^{-1}$ in the uniform fill mode. For a wide energy band used in EDD, these numbers must be multiplied by 10^3, so that, depending on the fill pattern, 10^7 to 10^5 photons fall on 1 mm^2 of the sample area within less than 100 ps. In the case of a wiggler source, these numbers are increased still by another order of magnitude. A fraction of the photons that are scattered by the sample pass through the receiving slit in front of the detector, and the question to be answered is that of the detecting system response to short bursts of photons arriving at regular intervals.

The functioning of the Ge detector is characterized by the length and shape of the output pulse of the amplifier, and by the operation logic of the ADC and MCA. The photons scattered from a given bunch arrive at the detector simultaneously, creating a single output pulse. Pulses that come from different bunches close to each other overlap partially, and the pulse height is increased from that of a single pulse. The effects are customarily described as dead-time losses and pulse pile-up. Detector electronics usually include the option for

automatic corrections for these effects, but the correction circuits have limited capabilities for handling very large pulse rates, and their actual effects on the output spectrum at the MCA may be obscure. The actual response of a Ge detector and pulse analyzing electronics can be found only experimentally, and the response function should be described by a model where the temporal structure of the incident radiation and time constants and operation mode of the detector electronics are properly included.

Fig. 2 shows the pulse shape at the amplifier output. The pulse is an asymmetric Gaussian (owing to charge collection time in the detector crystal), where the leading edge is slightly steeper than the trailing edge. Different shapes of the sum pulse from two photons arriving almost simultaneously are illustrated in the figure. The pulse sorting by the shaping amplifier and the ADC varies from one detector set-up to another, and here a widely used combination of an intrinsic Ge planar detector and an ADC is considered (Camberra 8715). When the pulse separation is sufficiently large, the sum pulse becomes double-peaked, and the detector electronics may assign the pulse according to the height of the first or the second peak, or count two separate pulses. The actual pulse pile-up can be illustrated by a simple model for the ADC: (i) when the minimum between two pulses is higher than the threshold, the sum of the pulses is detected (pile-up); otherwise they are detected separately. (ii) The peak height is defined when the signal falls by 10% (even if the signal rises again before falling below the threshold).

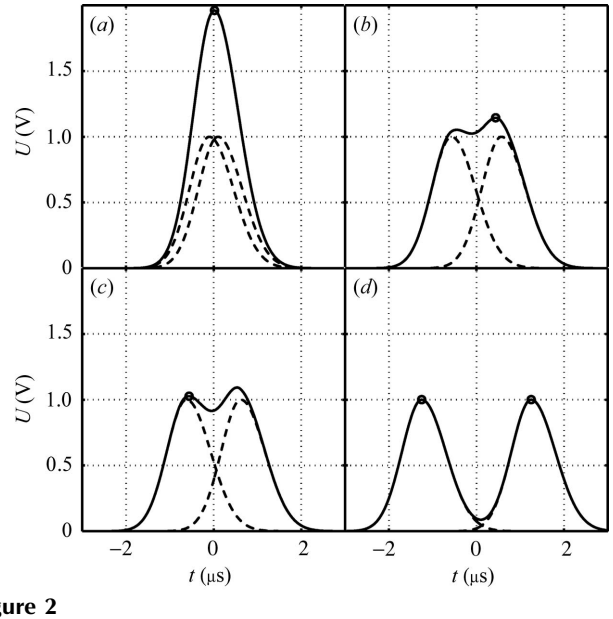

Figure 2
The output pulse of a Ge detector. The pulse shape is slightly asymmetric Gaussian, and different cases of the sum of two adjacent identical pulses are shown. The leading edge width is 0.48 μs, and the trailing edge width is 0.52 μs. The assigned pulse heights are indicated by small circles. In (*b*) and (*c*) the second maximum is higher than the first due to the asymmetric pulse shape. In (*a*) the almost simultaneous pulses are counted as a single pulse of double height; in (*b*) the signal has fallen less than 10% from the first peak value and the second maximum is recorded as the peak height; in (*c*) the fall is larger than 10%, and the first maximum is recorded as the peak height; and in (*d*) two separate peaks are recorded when the valley is lower than the threshold. Cases (*a*), (*b*) and (*c*) lead to dead-time loss, but also lead to pile-up signal between ε_0 and $2\varepsilon_0$, where ε_0 is the height of the single pulse.

For a continuous monochromatic source, the total amount of pile-up is

$$P_{\rm tot} = 1 - \exp\left\{-n_0\tau\left[2\ln(2U_0/U_{\rm T})\right]^{1/2}\right\},$$

and the n-event pile-up is

$$P_n = P_{\rm tot}^{n-1}(1 - P_{\rm tot}),$$

where τ is the shaping time of the amplifier, U_0 is the energy in volts and $U_{\rm T}$ is the threshold. For example, for n_0 = 50000 counts s^{-1}, τ = 0.5 μs, U_0 = 5.0 V and $U_{\rm T}$ = 0.1 V, the total amount of pile-up is 7.31% with P_2 = 6.77%, P_3 = 0.49% and P_4 = 0.04%. Because the effect of the filling mode on the total amount of the pile-up turns out to be very small and all count rates in this paper are well below 50000 counts s^{-1}, the effects of three or more event pile-ups on the calculated pile-up spectra are neglected.

For a pulsed source the probability that two successive photons are separated by m buckets is

$$p_m = \begin{cases} \dfrac{\left[1-\exp(-n_{\rm b})\right]^2}{n_{\rm b}N_{\rm occ}} \displaystyle\sum_{i=0}^{N_{\rm tot}-1} c_i c_{i+m} \exp\left[n_{\rm b}\left(1 - \sum_{k=i}^{i+m-1} c_k\right)\right], & m \neq 0 \\ 1 - \dfrac{\left[1-\exp(-n_{\rm b})\right]}{n_{\rm b}}, & m = 0, \end{cases} \quad (2)$$

where $n_{\rm b} = n_0\Delta T N_{\rm tot}/N_{\rm occ}$, n_0 is the total count rate, ΔT is the time between the buckets, $N_{\rm tot}$ is the total number of buckets, $N_{\rm occ}$ is the number of occupied buckets and c_i is the occupation number of the bucket (1 or 0). When $n_{\rm b}$ is small, the probability p_m is an autocorrelation function of the filling pattern.

The total pile-up spectrum is the sum of triple products,

$$n_{\text{p-u}}(\varepsilon) = \frac{1}{n_0}\sum_{ijm} p_m n(\varepsilon_i) n(\varepsilon_j) f\left[\varepsilon - E(\varepsilon_i, \varepsilon_j, m\Delta T, \tau)\right], \quad (3)$$

where the peak height $E(\varepsilon_i, \varepsilon_j, m\Delta T, \tau)$ in energy is calculated using the ADC model (ii). ε_i and ε_j are the energies of the successive photons separated by time $m\Delta T$, and $n(\varepsilon_i)$ and $n(\varepsilon_j)$ are their count rates, respectively. The sum over m runs until the two photons are detected separately using the ADC model (i). In the case of a modelled spectrum, f is the resolution function. For an experimental spectrum, the δ-function is used.

In order to give a flavour of what is to be expected in different cases, the pile-up distributions for typical fill patterns of the ESRF are shown in Fig. 3. For simplicity, only a single narrow energy band around ε_0 = 50 keV is considered. The pile-up is distributed between the nominal energy ε_0 and $2\varepsilon_0$. The operation mode of the detector electronics has particular effects, *e.g.* the cut-off of pile-up at 53 keV in the uniform fill mode is due to the transition from the case in Fig. 2(*b*) to that in Fig. 2(*c*). In the uniform fill mode, and in a partial fill mode (1/3 in this example), the pulses originating from closely spaced bunches combine to a sharp peak at $2\varepsilon_0$. On the other hand, combinations from bunches separated by 176 ns in the 16-bunch mode peak at many positions between ε_0 and $2\varepsilon_0$. The different intervals between two bunches give rise to nine

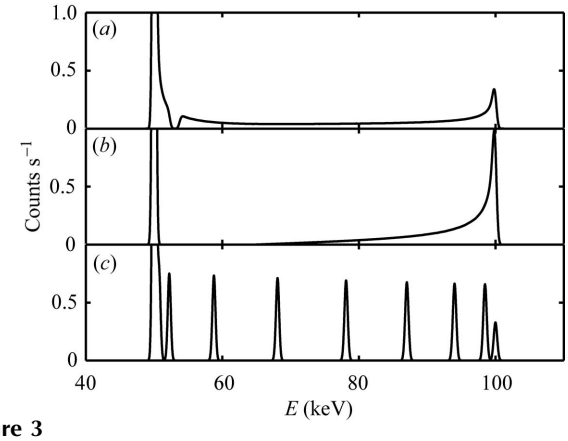

Figure 3
Pile-up distributions for different fill patterns of the ESRF storage ring: (*a*) uniform fill, (*b*) 1/3 fill, (*c*) 16-bunch mode with shaping time as in Fig. 2 and a count rate of 5000 counts s^{-1}. The integral of the pile-up distributions is about the same in all cases: 1.5%.

narrow peaks between ε_0 and $2\varepsilon_0$. Owing to the almost Gaussian shape of the detector output pulse, the distance between neighbouring peaks is not constant. Although the distributions are very different, the integral over the pile-up pulses is the same in all cases, irrespective of the fill pattern.

The actual pile-up distribution is very sensitive to the shape of the detector output pulse and the thresholds of the pulse-sorting logic. The observed positions and heights of the pile-up peaks are used for a precise determination of the shape of the detector output pulse, as discussed in detail in the next section.

3. EDD from a perfect crystal

EDD can be used for probing reciprocal space very efficiently. The direction of the scattering vector is determined by the incident and scattered beams, and EDD probes the reflectivity of the crystal along a line starting from the origin of the reciprocal space (Buras *et al.*, 1975). A challenging application is a measurement of the integrated intensities of a perfect crystal, because the crystal is totally reflecting within narrow energy bands, so that the count rates at these energies are those of the incident beam within these bands. When the crystal is oriented in such a way that the scattering vector passes through the reciprocal lattice point *hkl*, all allowed reflections *mh*,*mk*,*ml* are seen at multiple energies $m\varepsilon_{hkl}$. The Bragg law in the energy scale is given by

$$\varepsilon = \frac{hc}{2d_{hkl}\sin\theta} = \frac{12398\ \text{eV Å}}{2d_{hkl}\sin\theta}, \tag{4}$$

where ε is the photon energy, h is Planck's constant, c is the velocity of light, d_{hkl} is the lattice spacing and 2θ is the scattering angle. The situation is illustrated by the Ewald construction in Fig. 4. The scattering vector is $K = 2k_0\sin\theta = 4\pi\sin\theta/\lambda$, where λ is the X-ray wavelength, and the variation within the angular range $\Delta 2\theta$, determined by the receiving slit opening in the scattering plane, is $\Delta K = k_0\cos\theta(\Delta 2\theta)$. The range of total reflection is the Darwin width, which is independent of k_0 in the relative wavevector or energy scale,

$$\left(\frac{\Delta K}{K}\right)_{\rm D} = r_{\rm e}\frac{4d_{hkl}^2 K_{\rm pol,d}F_{hkl}}{\pi V_{\rm c}}, \tag{5}$$

as long as the dispersion corrections to the structure factor F_{hkl} are small. Here, $r_{\rm e}$ is the electron scattering length (classical electron radius), $K_{\rm pol,d}$ is the polarization factor in dynamical diffraction, and $V_{\rm c}$ is the unit-cell volume. The integrated intensity of a reflection from a non-absorbing perfect crystal is $(4/3)w_{\rm D}$, where the angular width of the total reflection is $w_{\rm D} = (\Delta K/K)_{\rm D}\tan\theta$. The number of photons diffracted to the receiving slit is

$$n_{hkl} = n_0(hkl)(4/3)w_{\rm D}, \tag{6a}$$

where $n_0 = (\mathrm{d}n_0/\mathrm{d}\varepsilon)_{hkl}\Delta\varepsilon$ is the number of incident photons (spectral flux) within the energy band accepted by the receiving slit, $\Delta\varepsilon = (1/2)\varepsilon\cot\theta\,\Delta(2\theta)$,

$$\begin{aligned} n_{hkl} &= \frac{2}{3}w_{\rm D}\left(\frac{\mathrm{d}n_0}{\mathrm{d}\varepsilon}\right)_{hkl}\varepsilon\cot\theta\Delta(2\theta) \\ &= \frac{2}{3}\left(\frac{\Delta K}{K}\right)_{\rm D}\left(\frac{\mathrm{d}n_0}{\mathrm{d}\varepsilon}\right)_{hkl}\varepsilon\Delta(2\theta). \end{aligned} \tag{6b}$$

The Darwin widths of perfect crystal reflections are accurately known, and even the integrated intensities for absorbing crystals can be calculated precisely. Accordingly, Bragg reflections from a perfect crystal can be used for determination of the incident spectral flux. However, count rates at ε_{hkl} are very large when synchrotron radiation is used, so that the detecting system response function must be known accurately.

When the incident spectrum and the efficiency of the detector are known, diffraction from a perfect crystal sample can be used to study the functioning of the detector under different conditions. Fig. 2 shows the simplest case, where the individual pulses have the same height, *i.e.* the pulses come

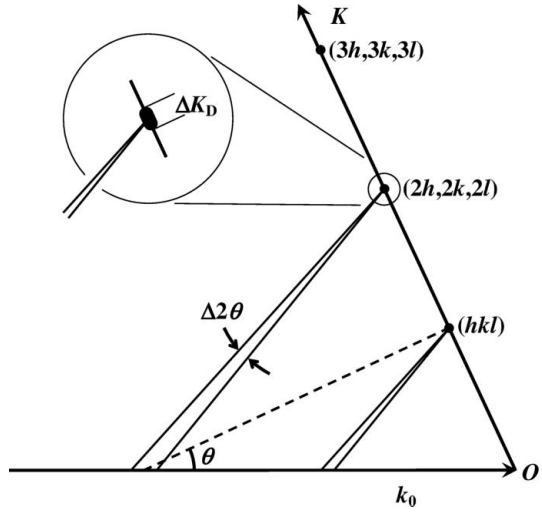

Figure 4
Ewald construction for energy-dispersive diffraction from a perfect crystal. The origin of the reciprocal lattice is indicated by *O*, and *K* is the scattering vector. The equatorial opening of the receiving slit is $\Delta 2\theta$, where 2θ is the scattering angle. When *K* passes through a reciprocal lattice point a range of energies is reflected, corresponding to the convolution of $\Delta 2\theta$ and the Darwin width of the reflection.

from the same reflection *hkl* but from different bunches of the synchrotron radiation beam. In general, the pulse heights correspond to ε_{hkl} and $\varepsilon_{h'k'l'}$, and the probability for the combination (hkl, $h'k'l'$) is proportional to the product of the integrated intensities of the respective reflections. Therefore, many combinations are possible, even though the small contribution of the background is ignored.

The initial parameters of the model for the operation of the Ge detector were taken from the manual supplied by the manufacturer, and the leading and trailing Gaussian pulse widths were refined by fitting the calculated pattern to the observed one. The pattern measured in the 16-bunch mode is most sensitive to the model parameters. A Si crystal wafer was oriented in symmetrical Laue geometry in such a way that the scattering vector passed through reciprocal lattice points $2m,2m,0$, where m is an integer (1, 2, 3, ...). Fig. 5 shows the energy spectrum of radiation scattered by the crystal from a wiggler beam, when the ESRF storage ring is operated in the 16-bunch mode. On the basis of Fig. 3, many 'extra reflections' are to be expected, not just the ones at energies $\varepsilon_{hkl} + \varepsilon_{h'k'l'}$, which would be seen with the uniform or a partial fill pattern. The observed pile-up pattern can be reproduced very closely by a calculation where the actual fill pattern and the optimized output pulse of the detector are used. The result is very sensitive to the pulse shape, which is fine-tuned for the best fit with the experimental diffraction pattern. The real Bragg reflections from the Si(hh0) crystal are indicated (sitting at the top of the pile-up fit), and it is seen that the very rich structure between the reflections is just due to pulse pile-up in the Ge-detector electronics.

The model for the detector operation was used to resolve the weak high-order reflections from Si(hh0), where the pulse pile-up is expected to have profound effects. The spectrum of the beam observed by the detector is shown in Fig. 6; the full spectrum on a logarithmic scale in the inset, and the part above 100 keV on an enlarged linear scale. In this case the measurements were carried out when the storage ring had the so-called 1/3 fill pattern. The upper curve shows the observed intensity, and the lower curve shows the pattern corrected for pile-up. The pile-up contribution follows exactly that shown in Fig. 3(*b*). The actual diffraction pattern is obtained when the pile-up distribution is subtracted, which leaves the reflections above a low background. There are some extra peaks about 11 keV below the low-order reflections. These are the so-called (K-edge) escape peaks of the detector, and they are assigned back to the peaks of their origin. At high energies the escape peaks are weak (here less than 1%), but at small energies they are substantial.

The relative Darwin widths and integrated intensities of the Si(hh0) reflections can be derived from (6), because the spectral flux and the detector response function are known from the measurements with calibrated powder samples (see the next section). The result is shown in Fig. 7 with calculated curves in the ideally dynamical and kinematical diffraction cases. The theoretical curves are obtained by using the formulae for the integrated intensity in symmetrical Laue diffraction and the analytical expression for the atomic scattering factor as a function of the scattering vector (Wilson & Prince, 1999). The effects of absorption and anomalous dispersion can be ignored in the present energy range. It is known that, at the limit where the crystal thickness is much less than the extinction length $\Lambda = V_c/(r_e\lambda K_{\rm pol,d}F_{hkl})$, the dynamical diffraction intensity approaches asymptotically the kinematical limit (Zachariasen, 1945). The present work may be the first case where this merge of theories is demonstrated

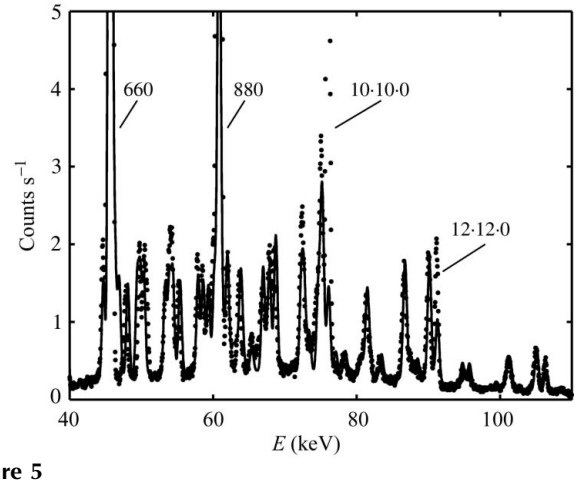

Figure 5
EDD pattern from a perfect Si(hh0) crystal, when the ESRF storage ring has the 16-bunch fill pattern. Radiation from the ID15 wiggler has been used, and the scattering angle 2θ is 24.4°. The solid line gives the pile-up pattern calculated from the detecting system response model. The shaping time is as in Fig. 2 and the total count rate is 13000 counts s^{-1}. Only a few of the maxima are due to the real Bragg reflections: 660 at about 46 keV, 880 at 61 keV and so on.

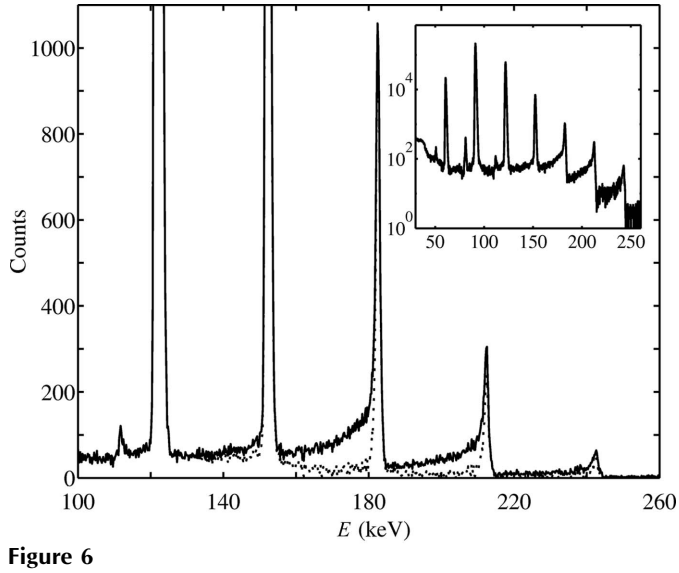

Figure 6
EDD pattern from a Si perfect crystal in symmetrical Laue geometry (2θ = 12.2°), when the scattering vector passes through the reciprocal lattice points ($2h,2h,0$). The storage ring has the 1/3 fill pattern, the shaping time is 0.5 μs, the total count rate is 11000 counts s^{-1} and the acquisition time is 180 s. The whole spectrum on a logarithmic scale is given in the inset, and the high-energy part is given on a linear scale. The upper curve (solid line) shows the recorded energy spectrum, and the lower curve (dotted line) shows the spectrum as corrected for the effects of pile-up. Note the small escape peaks about 11 keV below the low-order reflection peaks.

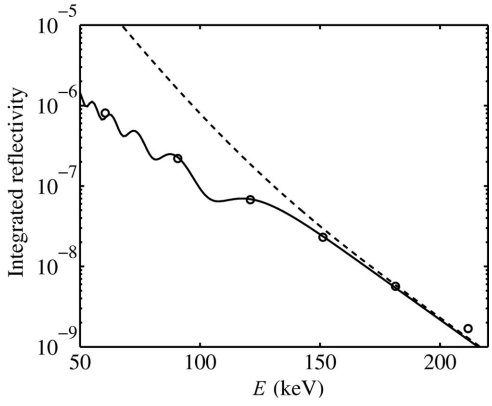

Figure 7
Calculated integrated reflectivity for the $(2h,2h,0)$ reflections of single-crystal Si according to kinematical theory (dashed curve) and to dynamical theory (solid curve; *cf.* Zachariasen, 1945). The measured points for reflections from 4,4,0 to 14,14,0 are indicated by the small circles.

by a simple experiment. The measured integrated intensities span three orders of magnitude, and in that range the difference between the kinematical and dynamical intensities decrease from two orders of magnitude to zero.

4. Powder EDD

Scattering of broad-band radiation from a powder sample includes many different components. In most cases the aim of the experiment is to separate the Bragg reflections from the total observed spectrum and, for that end, the profiles of the reflections and the components of the background must be described by an adequate model. There are some sum rules and internal relations for the integrated intensities of the reflections, the intensity of the thermal diffuse scattering, and the intensity of inelastic scattering. The relations are used to construct a self-consistent model for the total scattering, and the model is used for whole-pattern fitting introduced by the present authors (Honkimäki & Suortti, 1992*a*).

The different components of scattering can be calculated for an ideal powder sample of known structure and thermal motion parameters. The result is obtained on an absolute scale, and it can be used for determination of the spectrum of the incident radiation and the detector response function. The integrated scattered flux of reflection hkl to solid angle Ω at energy ε_{hkl} is

$$\begin{aligned}\int n_{hkl}(\varepsilon)\,\mathrm{d}\varepsilon &= n_{hkl}(\varepsilon_{hkl}) \\ &= \left(\frac{\mathrm{d}n_0}{\mathrm{d}\varepsilon}\right)_{hkl} \varepsilon_{hkl}\, A(\varepsilon) K_{\mathrm{pol,k}}(\Omega/4\pi)\, t(\varepsilon) d_{hkl}^3 \\ &\quad \times p_{hkl}(r_\mathrm{e} M_0 F_{hkl})^2. \end{aligned} \tag{7}$$

Here $(\mathrm{d}n_0/\mathrm{d}\varepsilon)_{hkl}$ is the incident photon flux per unit energy interval and $A(\varepsilon)$ is an attenuation factor, which includes absorption between the sample and detector, and the efficiency of the detector. $K_{\mathrm{pol,k}}$ is the polarization factor for kinematical diffraction, $t(\varepsilon)$ is the effective thickness of the sample (including absorption), p_{hkl} is the multiplicity of the reflection, and $M_0 = 1/V_\mathrm{c}$ is the number of scattering units (unit cells) in unit volume. When the diffraction pattern is recorded at low count rates, where the effects of dead-time and pulse pile-up are negligible, $(\mathrm{d}n_0/\mathrm{d}\varepsilon)A(\varepsilon)$ can be determined from a sufficient number of reflections. The method has been used successfully to calibrate the spectral brightness of different synchrotron radiation sources using well characterized standard samples. When the effective sample thickness and opening of the receiving slit are known, the spectral brightness is obtained in absolute units. The results were used for scaling the perfect crystal diffraction patterns discussed in the preceding section. One example of calibration of the source by the powder diffraction pattern is shown in Fig. 8 (Honkimäki & Suortti, 2001).

It is interesting to study the effects of fill patterns of a storage ring on powder diffraction patterns measured by an energy-dispersive detector. The excellent agreement between the experiment and calculation in the preceding section indicates that the response of the detector is accurately known. A simple case was chosen for detailed simulations of the diffraction pattern under different conditions. Fe has b.c.c. structure at room temperature, so that only reflections with $h + k + l = 2m$ are allowed, and the integrated intensities are calculated from (7). With a few exceptions, $h^2 + k^2 + l^2$ increases by steps of 2, so that in the ε^2 scale the reflections are at regular intervals. The calculated patterns of Fig. 9 demon-

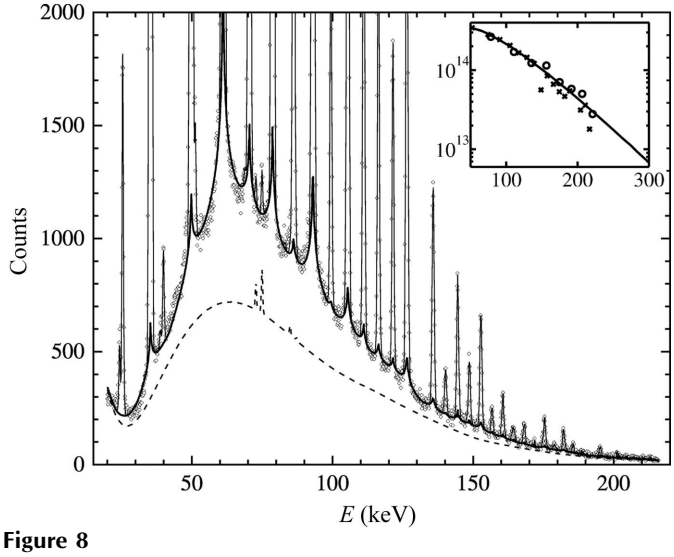

Figure 8
Whole-pattern fit to the EDD spectrum scattered from a standard Fe sample. The solid angle subtended by the detector is small in order to eliminate the effects of pile-up. The pattern includes the Bragg reflections, a function describing the thermal diffuse scattering, which peaks under the Bragg reflections and equals the part lost from the Bragg reflections due to thermal motion, Compton scattering, and parasitic Pb fluorescence from shielding. The total intensity of the background scattering is given by the thick line, and the inelastic part is indicated by the broken line. The spectral brightness [photons s^{-1} mrad^{-2} (0.1% bandwidth)$^{-1}$ (100 mA)$^{-1}$] of the radiation from the ID15 asymmetrical multipole wiggler (AMPW), as calculated using the integrated intensities of the Bragg reflections from Al (circles) and Fe (crosses) powder samples, is given in the inset. The solid line is calculated from source parameters, including the effects of beam filters.

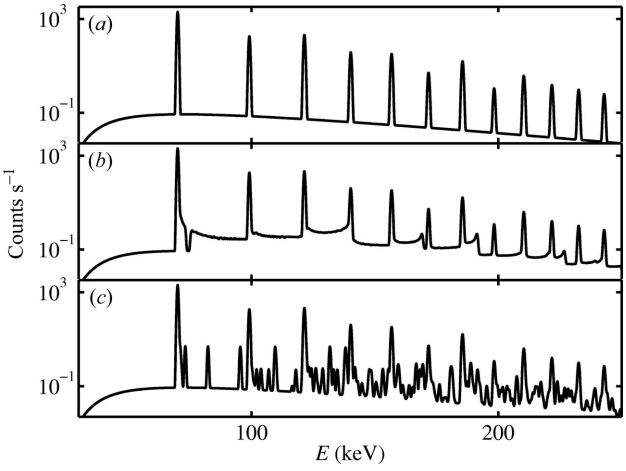

Figure 9
Simulated EDD patterns from an Fe powder sample, when different storage-ring fill patterns of the ESRF storage ring are assumed: (*a*) spectrum without pile-up and dead-time effects, (*b*) spectrum in uniform fill, and (*c*) spectrum in 16-bunch mode. The source is the AMPW of ID15 with the full field of 1.85 T. Symmetrical transmission geometry is used, the sample thickness is 1 mm, the scattering angle 2θ is 5°, the total count rate is 1.5×10^4 counts s^{-1}, and the shaping time of the amplifier is 0.5 μs. The total pile-up count rate is 910 counts s^{-1}. Background due to Compton scattering has been added.

strate that the ring fill pattern may introduce very rich structure between the proper reflections, particularly in the 16-bunch mode, and that the proper reflections are distorted.

The experimental situations simulated in Fig. 9 may be commonplace in cases where the fill pattern includes only a small number of widely separated pulses. The extra structure is regular, as seen in Figs. 3 and 9, and it may even be interpreted to be real, *e.g.* arising from multiple phases or superstructures in the powder sample. This is particularly clear in Fig. 9(*c*), where the simulated pattern from an Fe powder sample is shown for the 16-bunch fill pattern of the ESRF. It has to be emphasized that the total count rate is not particularly high, 1.5×10^4 counts s^{-1}, and that a short shaping time, 0.5 μs, is used in the calculation. In Fig. 9(*b*) the uniform fill pattern is used, and the effects of pulse pile-up are seen as increased background and distortion of the reflection profiles and integrated intensities. In truly accurate work there is no short-cut, but the pile-up must be calculated properly and subtracted from the pattern, or the pile-up pulse should be re-assigned to the contributing reflections.

5. Polycrystalline samples: applications in materials science

Materials of technological interest are often polycrystalline, resembling powder samples. However, the grain size is large in comparison with crystallites of ideal powder samples, and there may be strong texture and preferred orientation of the grains. Such a structure gives rise to a spotty angular pattern in diffraction of a monochromatic X-ray beam, or as strong variation in the EDD spectrum, depending on the orientation of the sample.

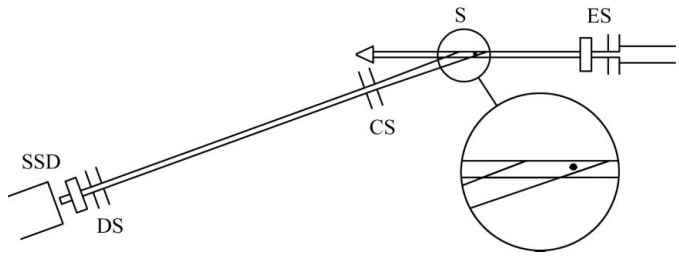

Figure 10
Experimental set-up for EDD measurement from a thick polycrystalline sample. The volume seen by the detector is determined by the beam width, the entrance slit ES, and the slits CS and DS in front of the solid-state detector (SSD). There may be only a small number of reflecting grains in the volume, and their non-uniform distribution causes variation in the actual scattering angle, as indicated by a spot in the enlarged picture of the scattering volume.

EDD has many advantages in studies of polycrystalline materials. The typical experimental set-up is shown in Fig. 10. For instance, the local texture in the scattering volume is obtained from the integrated intensities of a few reflections, which are recorded simultaneously when the sample is rotated about the incident pencil beam, or when a multi-detector in conical geometry is used. When the scattering angle is small, the reflections occur at high energies, which ensures that kinematical diffraction theory applies, and the scattering vector is almost perpendicular to the incident and reflected beams, which facilitates the analysis. To our knowledge, EDD has not been used in texture mapping, in spite of the obvious advantages.

A large and growing area of materials science applications of the EDD method is strain mapping and stress analysis. With an optimized set-up and adequate modelling of the EDD spectrum, the peak position changes $(\Delta\varepsilon/\varepsilon)_{hkl}$ have been determined with a precision of about 10^{-5} (Steuwer *et al.*, 2004). However, the actual accuracy, even in the relative values of $\Delta d/d$, may be an order of magnitude worse for two reasons. First, it is obvious that in order to find the true reflection profile the parasitic contributions to the EDD spectrum must be removed or eliminated and, for that, understanding the response of the Ge detector is essential. The pile-up spectrum distorts the reflection profiles as illustrated in Fig. 9. The positions of the reflections are shifted due to the pile-up, and the shifts depend on the total count rate at the detector, as shown in Fig. 11. In practice, the EDD pattern may vary strongly across the sample, so that a calculation of the pile-up distribution may not be feasible, and the only solution is to reduce the count rate to the level where the effects of pulse pile-up can be ignored. The counting statistics become the critical factor for determination of the position of a reflection, and the probable error can be calculated for a profile of Gaussian shape. Supposing that the background has been adequately removed, the relative statistical error in observed count rate y_i in the detector channel i is $y_i^{-1/2}$. The probable error $\Delta\varepsilon$ in the position of the whole profile is found by differentiating with respect to ε, yielding a simple result,

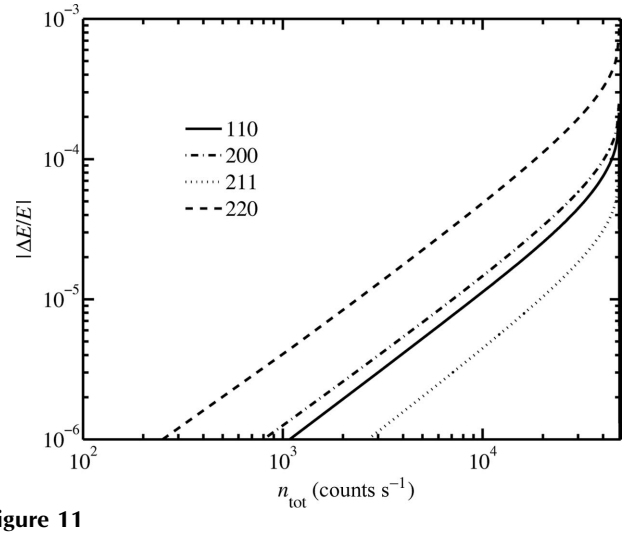

Figure 11
The absolute relative shifts of the positions of the first four reflections from an Fe powder sample as functions of the total count rate (*cf.* Figs. 9*a* and 9*b*). Uniform fill of the ESRF storage ring is assumed. The shift is positive ($0 < \Delta E$) for reflections 110, 200 and 211, and negative for 220. The positions are calculated from Gaussian fits to the reflection profiles.

$$\Delta\varepsilon = \sigma/n_{hkl}^{1/2}, \tag{8}$$

where σ is the standard deviation of the Gaussian, and $n_{hkl} = \Sigma y_i$ is the integrated number of counts in the reflection. For a Ge detector, $\sigma = a + b\varepsilon^{1/2}$, and, at $\varepsilon = 100$ keV, σ is about 200 eV, so that for $\Delta\varepsilon/\varepsilon = 10^{-4}$ the integrated count $n_{hkl} = 400$, but for $\Delta\varepsilon/\varepsilon = 10^{-5}$ already 40000 counts must be collected. It is seen in Fig. 11 that on that level of accuracy the total count rate should be less than 2×10^3 counts s^{-1}, and an order of magnitude less for one reflection. In our example the acquisition time should be 200 s. The second limitation in the accuracy is due to the detector electronics, because maintaining long-term stability within 1 eV over the whole counting chain may be impossible. Moreover, the channel width of an MCA for an energy range of 100 keV is typically 25 eV, preventing monitoring the stability by a pulse generator on the 1 eV level.

6. Summary

EDD is a very powerful tool for studying crystal structures, and, in particular, their changes under extreme conditions. When synchrotron radiation is used, the data acquisition times become very short making dynamical studies possible. However, the detecting system response to high rates of diffracted photons of different energies and arriving in short bursts is rather complicated. The effects are usually called pulse pile-up and detector dead-time, but these depend on the time structure of the X-ray source and on details of the detector electronics functioning. These can be modelled accurately and the model can be used to resolve energy spectra that include many artefacts arising from pulse pile-up. It is concluded that without an adequate correction for these effects the results obtained by EDD remain qualitative or even questionable.

In this work we have reported results for EDD, obtained with a commonly used Ge detector and standard electronics. However, the pulsed time structure of the synchrotron radiation source introduces a structured pile-up distribution in the output of any photon-counting detector. This may be invisible, or can be accounted for by a simple correction for dead-time loss, but it is always advisable to study how the detector and associated electronics function, and simulate the output under the actual experimental conditions. There is no simple recipe for making the pile-up corrections by extrapolating from the present examples. The results give some guidelines, but for actual corrections a realistic model for the detector operation must be used.

The authors thank K.-D. Liss for providing the diffraction spectrum of the Si(*hh*0) crystal, measured during the 16-bunch operation of the ESRF storage ring.

References

Buras, B., Staun Olsen, J. & Gerward, L. (1976). *Nucl. Instrum. Methods*, **135**, 193–195.
Buras, B., Staun Olsen, J., Gerward, L., Selsmark, B. & Lindegaard Andersen, A. (1975). *Acta Cryst.* A**31**, 327–333.
Giessen, B. C. & Gordon, G. E. (1968). *Science*, **159**, 973–975.
Hall, C., Barnes, P., Cockcroft, J. K., Colston, S. L., Häusermann, D., Jacques, S. D. M, Jupe, A. C. & Kunz, M. (1998). *Nucl. Instrum. Methods*, B**140**, 253–257.
Honkimäki, V. & Suortti, P. (1992*a*). *J. Appl. Cryst.* **25**, 97–104.
Honkimäki, V. & Suortti, P. (1992*b*). *J. Appl. Cryst.* **25**, 105–108.
Honkimäki, V. & Suortti, P. (2001). *Defect and Microstructure Analysis by Diffraction*, edited by R. L. Snyder, J. Fiala and H. J. Bunge, pp. 41–58. Oxford University Press.
Jupe, A. C., Turrilas, X., Barnes, P., Colston, S. L., Hall, C., Häusermann, D. & Hanfland, M. (1996). *Phys. Rev. B*, **53**, 14697–14700.
Laundy, D. & Collins, S. (2003). *J. Synchrotron Rad.* **10**, 214–218.
Mao, H. & Hemley, R. J. (1998). *Rev. Mineral.* **37**, 1–32.
O'Hare, D., Evans, J. S. O., Francis, R. J., Shiv Halasyamani, P., Norby, P. & Hanson, J. (1998). *Micropor. Mesopor. Mater.* **21**, 253–262.
Parrish, W. & Hart, M. (1988). *Austr. J. Phys.* **41**, 403–411.
Prewitt, C. T., Coppens, P., Phillips, J. C. & Finger, L. W. (1987). *Science*, **238**, 312–319.
Pyzalla, A., Camin, B., Buslaps, T., Di Michiel, M., Kaminski, H., Kottar, A., Pernack, A. & Reimers, W. (2005). *Science*, **308**, 92–95.
Steuwer, A., Santisteban, J. R., Turski, M., Withers, P. J. & Buslaps, T. (2004). *J. Appl. Cryst.* **37**, 883–889.
Wilson, A. J. C. & Prince, E. (1999). Editors. *International Tables for Crystallography*, Vol. C. Dordrecht: Kluwer.
Zachariasen, W. H. (1945). *Theory of X-ray Diffraction in Crystals.* New York: John Wiley.